Canelles landslide: modelling rapid drawdown and fast potential sliding

Núria M. Pinyol, Eduardo E. Alonso, Jordi Corominas & José Moya

Landslides
Journal of the International Consortium on Landslides

ISSN 1612-510X
Volume 9
Number 1

Landslides (2012) 9:33-51
DOI 10.1007/s10346-011-0264-x

Springer

Original Paper

Landslides (2012) 9:33–51
DOI 10.1007/s10346-011-0264-x
Received: 30 November 2010
Accepted: 12 April 2011
Published online: 17 May 2011

Núria M. Pinyol · Eduardo E. Alonso · Jordi Corominas · José Moya

Canelles landslide: modelling rapid drawdown and fast potential sliding

Abstract A large landslide ($40\times10^6 m^3$) was reactivated on the left bank of Canelles reservoir, Spain. The instability was made evident after a considerable reduction of the reservoir level. The drawdown took place during the summer of 2006 after several years of high water levels. The drawdown velocity reached values between 0.5 and 1.2m/day (registered at low elevations). The paper reports the geological and geotechnical investigations performed to define the movement. The geometry of the slip surface was established from the detailed analysis of the continuous cores recovered in deep borings and from limited information provided by inclinometers. Deep piezometric records provided also valuable information on the pore water pressure in the vicinity of the failure surface. These data allowed validating a flow–deformation coupled calculation model, which takes into account the changes in water level that occurred 4 years previous to the failure as well as the average rainfall. The analysis indicates that the most likely reason for the instability is the rapid drawdown that took place during the summer of 2006. The potential sudden acceleration of the slide is also analysed in the paper introducing coupled thermal hydraulic and mechanical effects that may develop at the basal shearing surface of the sliding mass. The results indicate that the slide velocity may reach values around 16m/s when displacement reaches 250m.

Keywords Landslide · Analysis · Modelling · Finite elements · Stabilisation · Rapid drawdown · Fast sliding

Introduction

The Canelles dam, a 151-m-high double curvature arch structure, creates one of the largest reservoirs in Spain (maximum storage volume 560 Hm^3) (Fig. 1). The dam was built in the period 1958–1962 and therefore a long time record of reservoir elevation is available. The dam was designed with several objectives: hydrologic regulation of the Noguera Ribagorçana river, land irrigation, water supply to the lower reach of the river basin and power generation.

Water demands and rainfall intensity in the watershed control the evolution of water elevation in the reservoir. Figure 2 shows the recorded absolute elevation in the period 1987–2009. As a reference, the maximum water elevation in the reservoir is 506 m. The elevation of dam crest is 508 m. The significant decrease of annual rainfall in the period 2005–2006 resulted in a considerable reduction of the average water level (Fig. 2). In addition, irrigation demands in spring and summer resulted in additional water level reductions. During the summer of 2006, the drawdown velocity reached values of 1.2 m/day in the first days of August. This is a high rate of drawdown in general terms except for reservoirs associated with reverse pumping schemes.

At a certain point during the summer of 2006, a large landslide was reactivated on the left bank of the reservoir (Fig. 1b). The first indication of instability was the development of a long continuous tension crack (Fig. 3) whose opening varies between 0.1 and 0.3 m. Subsequent investigation, reported in this paper, led to an estimation of the landslide volume of around 40×10^6 m^3. The magnitude of the landslide and its potential for sudden acceleration were of special concern for the reservoir owners and state authorities. Several questions were put forward. They referred to the reasons for the landslide development, its likely evolution, the relationship between reservoir operation and landslide motion, the risk of a fast sliding and its consequences and the implications for the management of the reservoir in the future.

This paper reports the main conclusion of the geological and geotechnical investigations performed and the set of analyses carried out. It also provides an answer to the questions raised. At the time of writing the manuscript, the Canelles slide is essentially stable and the proposed stabilisation measures are being designed. The Canelles slide is an interesting case of landslide reactivation induced by a fast drawdown. It also allowed applying some recent developments concerning the explanation and the prediction of fast sliding. They explain the potential high velocity of the landslide by the coupled thermal hydraulic and mechanical effects which may develop at the basal shear surface. These developments have been described in some recent papers (Vardoulakis 2002; Pinyol and Alonso 2010a, b).

Geology

The Canelles dam and landslide are located at the Blancafort Sierra in the outer Pyrenean ranges (Fig. 4). The uplift of the Pyrenees during the Alpine orogeny was associated with thrusting and displacement of large nappes (Upper Thrust Sheets) that covered distances of more than 150 km southwards (Fig. 4a). The Blancafort Sierra is outer zone of the range, located just south of a main thrust front (the Montsec Sierra thrust front, Fig. 4b).

The emplacement of the nappes was accompanied by parallel folding of the strata. Main folds show wavelengths of several kilometres. The Blancafort Sierra forms the northern flank of the Canelles anticline and its foot ends in the Blancafort syncline (Fig. 4b). Development of parallel folds during the orogeny involved slipping on bedding surfaces and, consequently, a reduction of the shear strength of these surfaces.

The local geology of the Canelles landslide was established by air photo interpretation, by field mapping and by interpreting 16 borehole logs (Fig. 5).

The bedrock outcropping in the area consists of a sequence of sedimentary rock units that correspond to the transit of the Upper Cretaceous to the Lower Paleocene. The stratigraphic column is from bottom to top:

(a) Lower grey limestones: grayey limestones of lacustrine origin interbedded with grey marls of Campanian to Maastrichtian age. A minimum unit thickness of 40 m.
(b) Grey sandstones: predominantly medium to coarse grained sandstones of grey and ochre colour, interbedded with thin layers of multicoloured (grey, red, ochre) clayey siltstones, sandy siltstones and conglomerates of Maastrichtian age. Observed unit thickness between 35 and 55 m.
(c) Clayey limestones: thin layer of grey and white limestones and marly limestones that appear only locally (boreholes

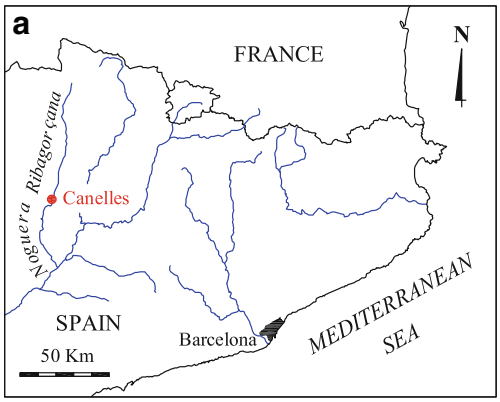

Fig. 1 **a** Ubication of the Canelles reservoir in Catalunya (Spain); **b** location of the reservoir, the dam, the Blancafort Sierra and the non-submerged limit of the slide under study (in *yellow*). To the south of the slide, the northern slope of Blancafort Sierra, presents a well-developed drainage network on a rock substratum (cemented marls and sandstones), showing no additional failure scars

cross section III, Fig. 5) and of Maastrichtian–Lower Paleocene age. Maximum observed unit thickness of 10 m. This area does not outcrop in the area represented in Fig. 5.

(d) Red claystones: clayey siltstones and silty claystones reddish and ochre coloured of continental origin. Locally interbedded with thin limestone and marly layers 1–2 m thick. Lower Paleocene age (Garumnian facies). The thickness of the unit ranges usually between 2 and 12 m, though occasionally reaches 33 m.

(e) White limestones: massive grey to white limestone layer having either micritic or brecciated facies, the latter with silty or clayey multicoloured matrix (reddish, grey, ochre, brown) of Paleocene age (Garumnian facies). Thickness of the unit between 15 and 25 m.

(f) Siltstones and limestones: heterogeneous unit composed of clayey silts and siltstones, silty clays and multicoloured calcareous marls, which are predominant and layers of calcarenites, micritic limestones and brecciated limestones. Lower Paleocene age (Garumnian facies). The minimum thickness of this unit is 70 m.

At the northern slope of the Blancafort Sierra, layers are arranged in a WNW-ESE direction, dipping northward. Dip angles changes from 45°, at the upper part of the slope, to horizontal at the bottom of the slope. The core of the Blancafort syncline outcrops at the lowest part of the slope, where the layers dip slightly (8° on average) to the South, that is, in an upslope direction.

Characterization of the Canelles landslide

In order to proceed with the analysis of the stability of the Canelles landslide and its potential for catastrophic acceleration, the reconnaissance work has been oriented to: (a) identify the mechanism of the landslide, (b) define the geometry and magnitude of the potentially movable mass, (c) determine the mechanical and hydraulic properties of the materials involved and (d) establish the groundwater regime of both the slope of the Blancafort Sierra and the landslide.

The reconnaissance work included a campaign of 20 boreholes, 4 of them equipped with vibrating piezometers and 9 with inclinometric casings (see Fig. 5).

Landslide mechanism

The upper part of the Canelles landslide is delimited by a continuous peripheral tension crack, which may be easily identified at field, and by non-submerged lateral boundaries established with reasonable accuracy on the basis of existing cracks and further morphological features (Figs. 4 and 5). The

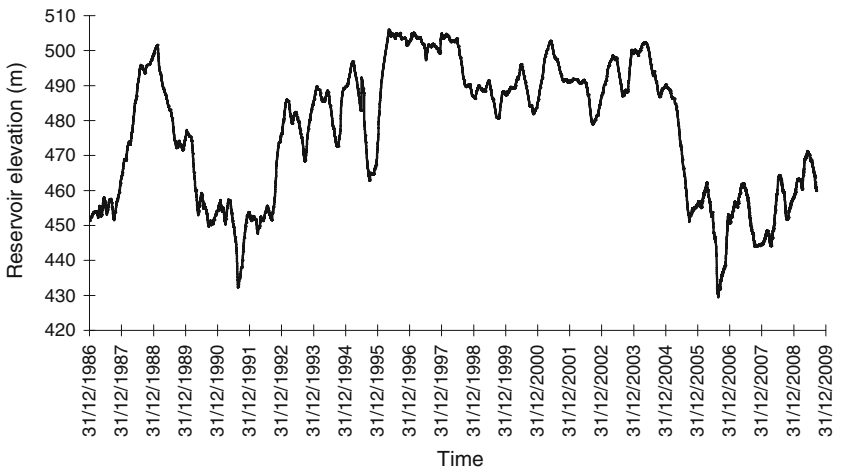

Fig. 2 Evolution of water elevation in the reservoir

Fig. 3 Tension crack developed in August 2006 that defines the upper boundary of the slided mass

back crack of the landslide has a length of 1.2 km and it is roughly parallel to the bank of the reservoir. The long tension crack developed at the foot of a continuous scarp 4–5 m high (Fig. 6). The presence of the mentioned tension crack along with the absence of tilting in the adjacent ground surface suggests a translational movement. The slide progresses northward into the reservoir. The lower part of the slide is submerged and it is more difficult to locate its boundary. It was assumed to coincide with an abrupt decrease of the slope angle, near the former alluvial plain of the river.

Evidences for slope instability outside the landslide area, mapped in Fig. 5, were specifically searched. However, neither activity features (cracks, scars) nor slide deposits were found at higher elevations of the Blancafort Sierra, which limits the landslide on its southern side. The Blancafort Sierra presents a well-developed and regular drainage network on stable bedrock sandstones and limestones. The development of such a drainage network must have required a long period to form so it can be concluded that the landslide is confined by the mentioned tension crack. Furthermore, the lateral continuity of bedding planes in the bedrock outcropping at the upper slope of the Blancafort Sierra was also observed; the absence of bedding disruption was judged as an additional indication of stability of this part of the slope.

No historic records of landsliding activity on this area are available, but the geomorphic evidences found suggest that the movement observed in August 2006 was a reactivation of a dormant translational slide. Aerial photographs taken in 1956 show already the presence of this scarp.

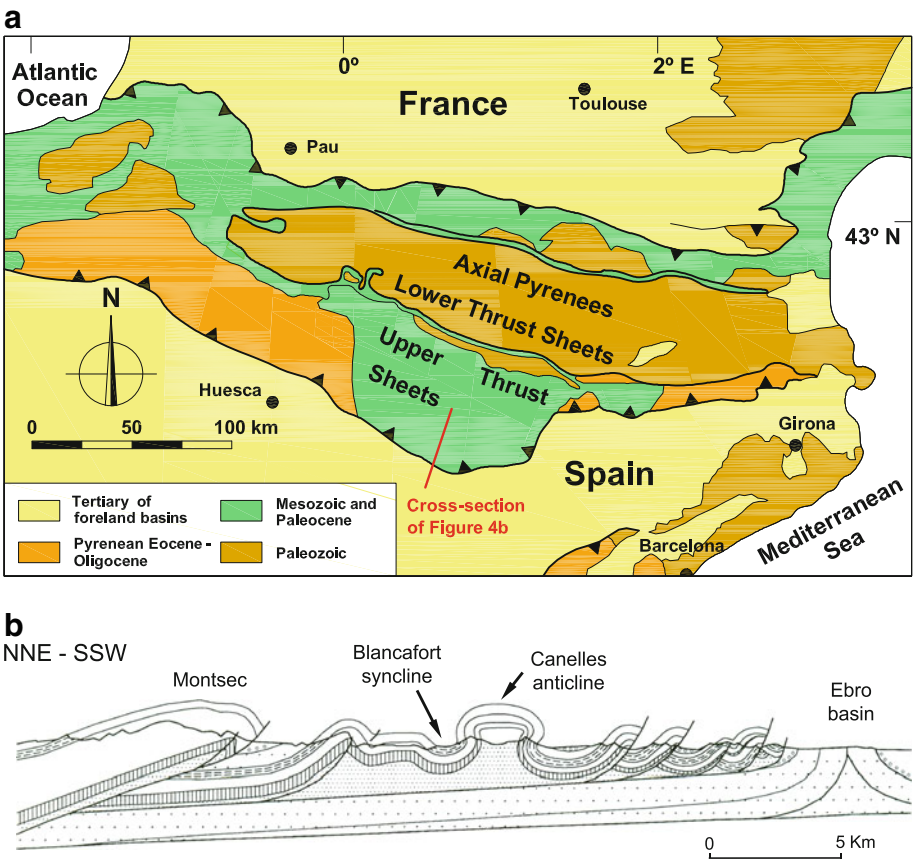

Fig. 4 Geological setting of the Canelles landslide. **a** Tectonic map of the Pyrenees with main thrust systems (modified from Vergés 1993). **b** Geological cross section of the outer Pyrenean Sierras in which both the Canelles anticline and Blancafort syncline are located (from Martínez Peña and Pocoví 1988); the location of the cross section is shown in **a** by the *red line*

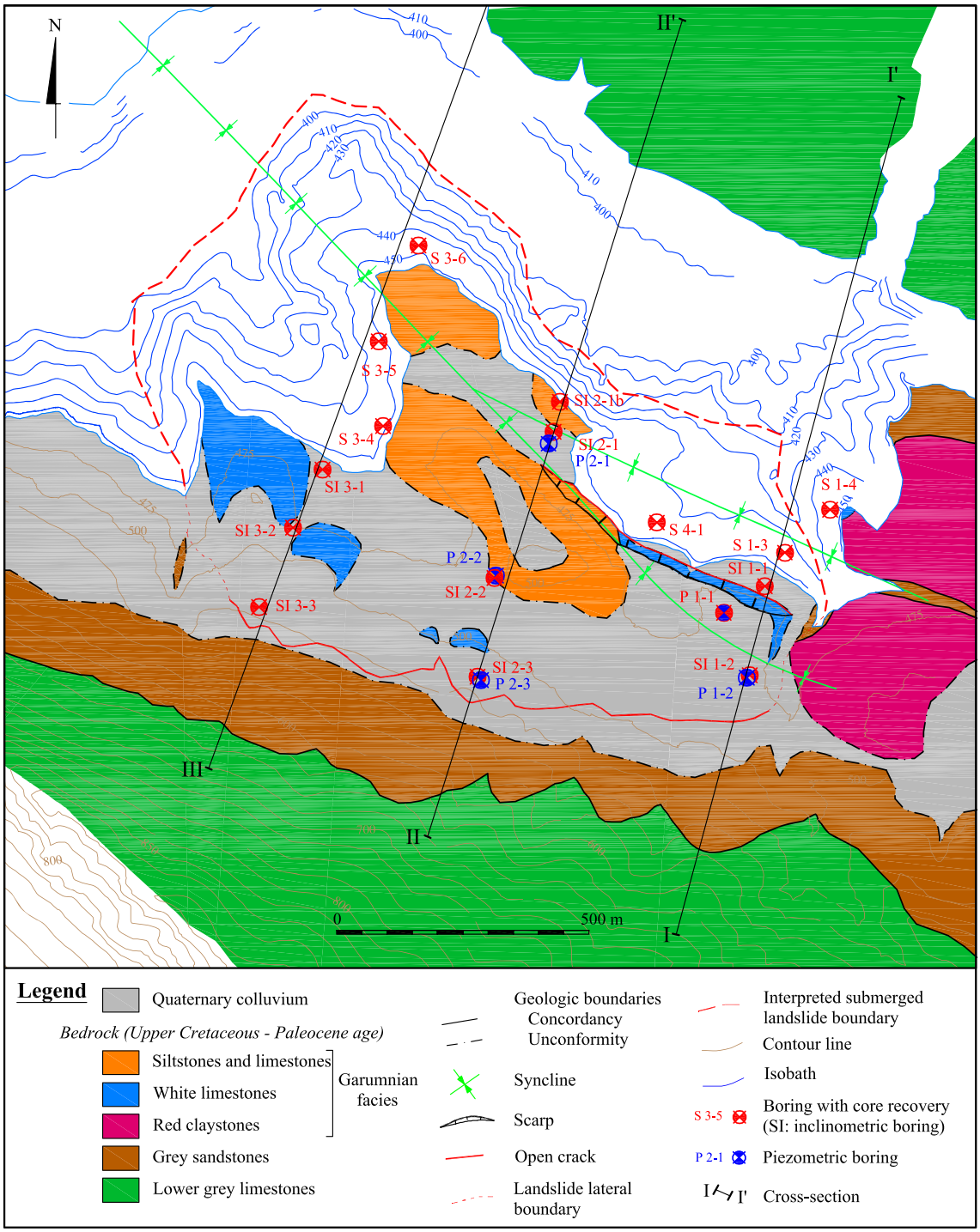

Fig. 5 Detailed geological map of the Blancafort Sierra and the Canelles landslide. The location of boreholes, inclinometric casings (i.e. SI 1-1) and piezometers (i.e. P 1-2) is also shown. *Dashed red line* marks the submerged boundary of the landslide

Landslide geometry: location of the sliding surface

The location of the sliding surface should be ideally obtained from the interpretation of the inclinometric measurements. All nine inclinometers reached significant depths (100 to 140 m) well beyond the expected slip surface and were anchored on stable ground. First readings were made on February 2007. Most of the inclinometer measurements, however, remained within the resolution of the instrument, and they could not provide a reliable and systematic indication of the position of the sliding surface. At some locations (Fig. 7), a sliding plane could be identified but this case was the exception rather than the rule. It was concluded that the slide remained essentially stable after the development of the long peripheral crack in the summer of 2006. The alternative to locate the sliding surface was to perform a detailed examination

Fig. 6 Scarp marking the crown of the slide (highlighted by the *yellow lines*). The tension crack shown in Fig. 3 is located at the foot of this scarp

of the recovered drill cores searching for reliable criteria to identify the position of the sliding surface.

Given that the observed mechanism is a translational failure and that the layers in the vicinity of the landslide show small dip angles, the working hypothesis has been that the slip surface must have developed parallel to the strata, along a weak layer. Failure across weak and sound rock was not discarded but was found less feasible.

The presence of shear surfaces is often assumed as evidence of slip plane (i.e. Hutchinson and Bhandari 1971; Hutchinson 1983; Alonso et al. 1993; Moya 2004; Corominas et al. 2005). In the sequence of materials of the Blancafort Sierra, either slickensided or striated surfaces are features that are found in all the lithological units. The presence of these surfaces is interpreted as the result of relative displacements among strata during folding and the emplacement of the Alpine nappes. Even though it is expected that the slip surface of the Canelles landslide may re-use one or more pre-existing (inherited) shear surfaces for its development, most of them are not related at all to the landslide.

The identification of the slip surface of the landslide was finally based on the simultaneous occurrence of a few landslide-associated features which are summarized as follows:

- Presence of frequent shear planes. These planes can be easily identified due to the existence of slickensides or polished surfaces.
- Continuity and parallelism of shearing planes with respect to the potential sliding plane.
- Degree of core recovery and quality of the strata above the shear plane. The movement is expected to break the most rigid strata and produce a weaker and fractured rock mass when compared with the intact rock layers.
- Correlation with inclinometric records wherever possible.

Finally, the interpolation of the slip surface between boreholes must show a consistent geometry.

Figure 8 provides a graphic account of this procedure applied to borehole S 3-5. Figure 9 shows an outcrop of the multicoloured clays of the Garumnian facies (red claystone unit) on the eastern side of the slide. They were exposed by a deep gully cutting the bedrock. Two block samples were taken in this outcrop for further testing in the laboratory. Striated polished surfaces within this Garumnian clay were also systematically recovered in borings as shown in Fig. 10.

Three geological cross sections, in the position shown in Fig. 5, were prepared. They are shown in Figs. 11, 12 and 13. The position and length of all the borings performed are indicated in the figures. Strata are gently tilted and define a large syncline structure. The sliding surface is located in the continuous and relatively thin red claystone unit.

Geomechanical and hydraulic properties of the Garumnian clay

Block samples were tested in the Geotechnical Laboratory of UPC. The results given below correspond to the four specimens tested. Natural densities ranged between 17.1 and 18.8 kN/m^3. Water content was close to 20%. Calculated void ratios (0.96–0.68) are high, probably a consequence of the natural unloading and partial weathering of the exposed outcrops of Garumnian clay. The clay was classified as high plasticity clay (w_L=54–57%, PI 26–31%). The clay content was close to 40% in all cases.

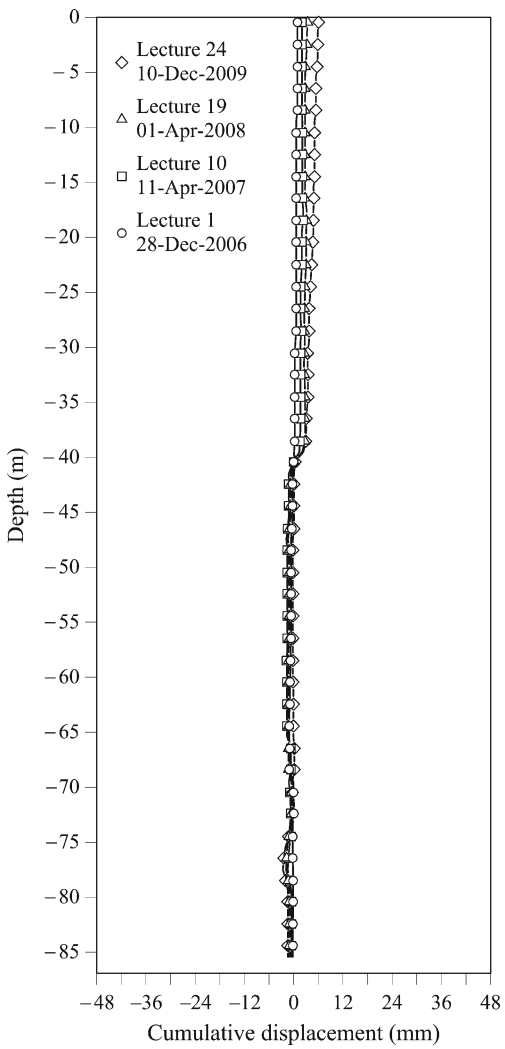

Fig. 7 Measured data on inclinometer installed in boring SI 3-1

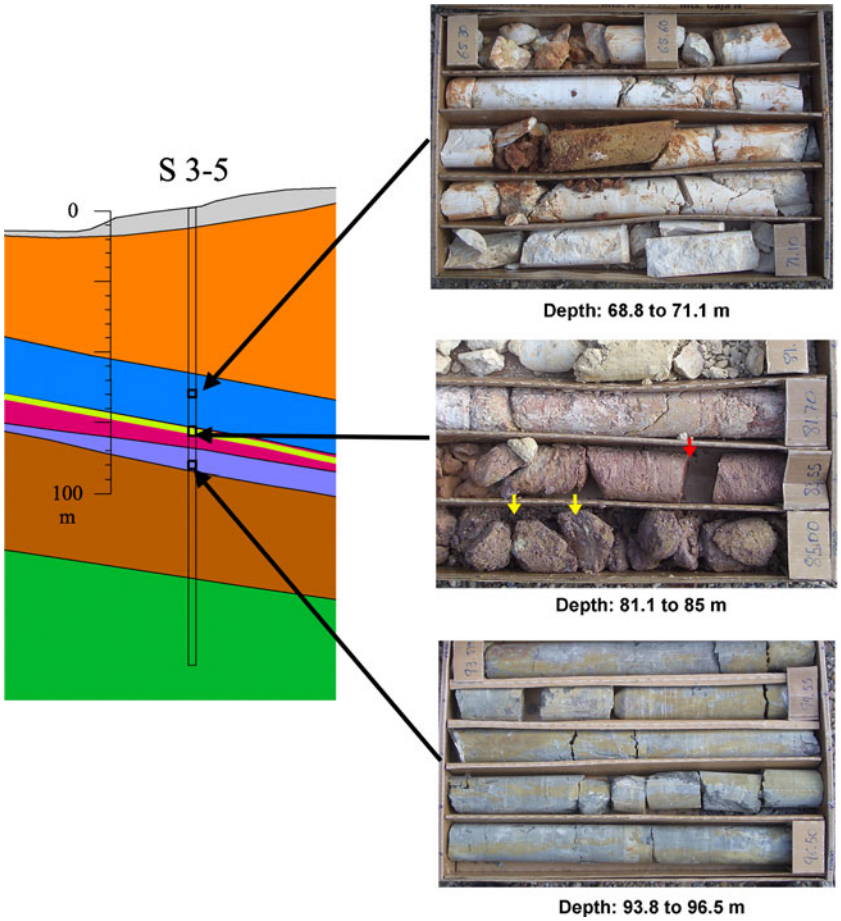

Fig. 8 Sliding surface identified by the presence of striated surfaces in the Garumnian clay between depths 81.1 and 85.5 m in borehole S 3-5 (marked by *small arrows* in central photograph). The *red arrow* on this photograph indicates the location of the shear surface shown in Fig. 10b. Above these depths, bedrock cores (siltstones and limestones) show a low quality (upper photograph); high quality samples were recovered from the sandstones and limestones that underlay the Garumnian clay

Since the slide was a reactivation of an ancient failure, residual strength conditions will be acting on the sliding surface. Ring shear tests on remoulded specimens provided the strength envelopes shown in Fig. 14. A residual friction angle of 12–13° was determined for the range of effective vertical stresses 100–250 kPa. The sliding surface is often located at depths of 50–100 m, and therefore, normal effective stresses prevailing "in situ" are substantially higher (800 kPa in average) than the testing range. In addition, past normal stresses, both of lithostatic and tectonic origin, may have reached also higher than the present values. Therefore, in situ friction angle at the failure surface are probably smaller than the values given in Fig. 14. A likely in situ value is estimated at φ'_{res}=10–12° (Stark and Eid 1994; Alonso 2005).

Fig. 9 Outcrop of the red-wine Garumnian clays

The clay permeability was measured under a stress of 300 kPa in an oedometer cell by a stationary flow method. Two undisturbed specimens provided $k=4.2\times10^{-10}$ and 4.9×10^{-11} m/s. This set of results will guide the selection of parameters in the analysis performed.

Piezometric response in the vicinity of the sliding surface

Figures 11, 12 and 13 show the water level of the reservoir at some specific times.

The development of the continuous crack at the ground surface in the summer of 2006 occurred when the water level in the reservoir reached elevation at 430 m, which is the minimum value since 1987 (Fig. 2). Note also that in the years previous to 2005, the reservoir level was maintained at elevation of 490±5 m.

Fig. 10 Striated and polished surfaces within Garumnian clays recovered in borings **a** S 3-6 (depth 89.1 m) and **b** S 3-5 (depth 84 m, see location in Fig. 5)

Hydrologic conditions in the slide, even in strata of low permeability such as the Garumnian clay, prior to the continuous and strong decrease in levels during 2005 and 2006 were most likely controlled by the long period of high water levels. It is implied that stationary conditions associated to a water elevation of 490±5 m would have developed for the entire stratigraphic sequence.

Figure 5 indicates the location in plan view of the vibrating wire piezometers installed. Several pressure sensors (three or four) were installed in each borehole at different depths. Pressure sensors were installed around the red claystone layer where the failure surface was most likely located.

Piezometer records are shown in Figs. 15, 16, 17, 18 and 19. The recorded water pressures in the sandstone stratum follow the water level elevation in the reservoir. The response is fast in all the piezometers except for the piezometers located in P 2-3. On the contrary, the piezometers located in the claystone layer maintain high pressures, which in some cases exceed the pressures corresponding to the current water reservoir elevation. Note, in particular, the value of the pressures recorded in P 1-2 and P 2-2 in the piezometer located within the clayey Garumnian stratum. The pressure in this case remains constant and independent to the water level elevation. This result confirms the low permeability of the clay stratum, in contrast to the higher permeability of the sandstone and limestones underneath. The pressure in the upper part of the slide (P 2-3) seems not to be directly connected to the reservoir. High pressure values are measured in all rock layers (Fig. 18). These values of water pressure probably are a consequence of direct infiltration from rainfall or perhaps the result of other sources of water, not well defined, linked to the geological structure of the area.

As a summary, the examination of piezometer measurements leads to the following conclusions:

- The hydraulic behaviour of the Garumnian clay (red claystone unit) seems to be independent from the underlying sandstone unit.
- The pressures in the sandstone stratum, except for the upper part of the slide, follow immediately the water level elevation in the reservoir. This behaviour is an indication of the high permeability of the sandstone.
- Pressures remain essentially constant in the Garumnian clay and independent from water elevation mainly during the first 7 months of measurements when reservoir elevation was lower than 460 m. This is an indication of the difficulty to dissipate or increase water pressures within clayey layers where the sliding surface is located. It also points out the low "in situ" permeability of this clay level.

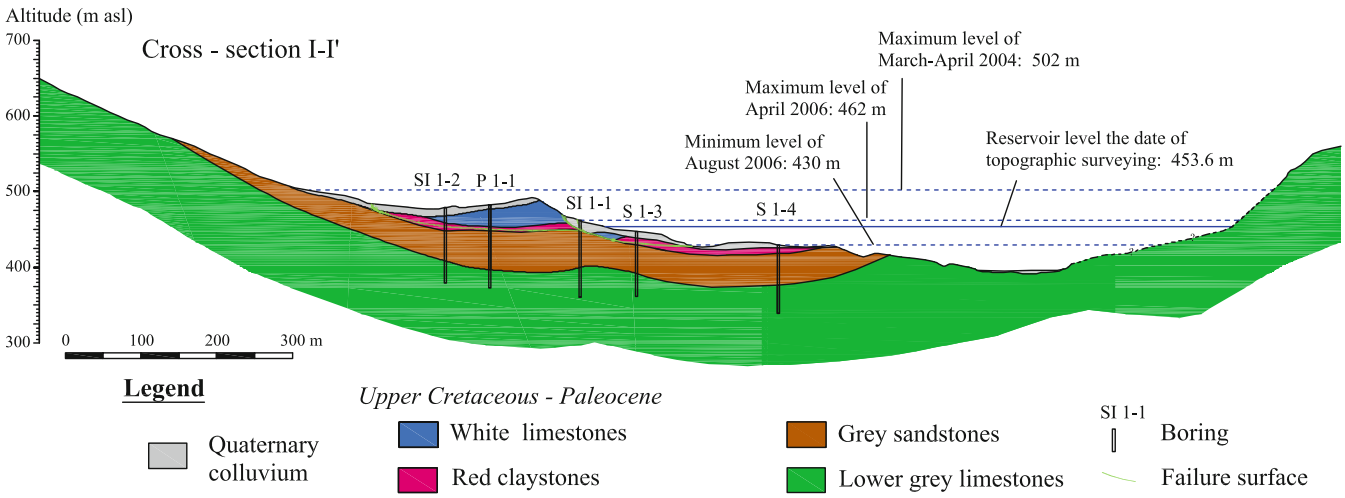

Fig. 11 Geological cross section I (see location in Fig. 5)

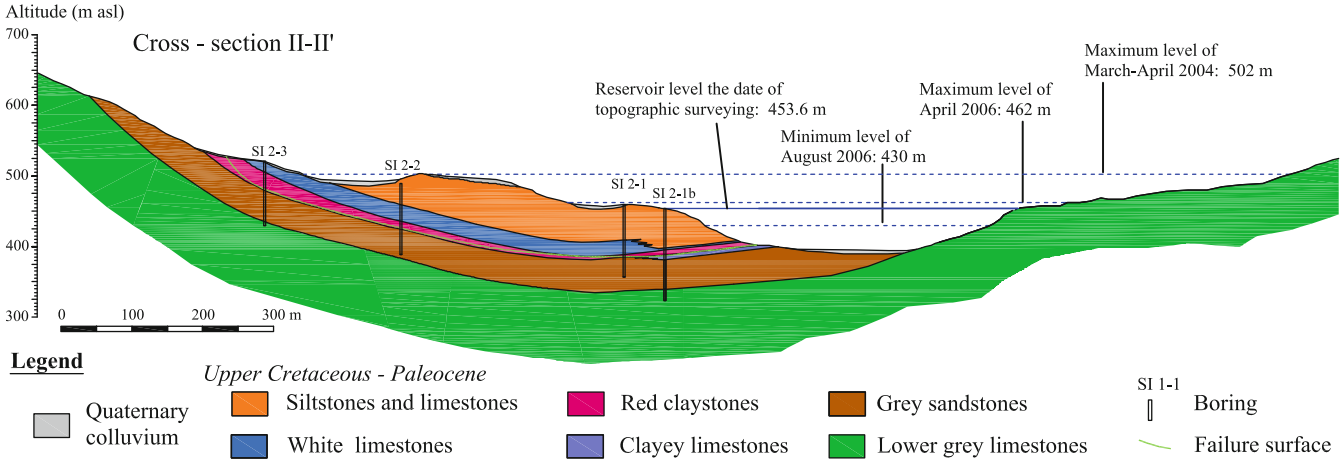

Fig. 12 Geological cross section II (see location in Fig. 5)

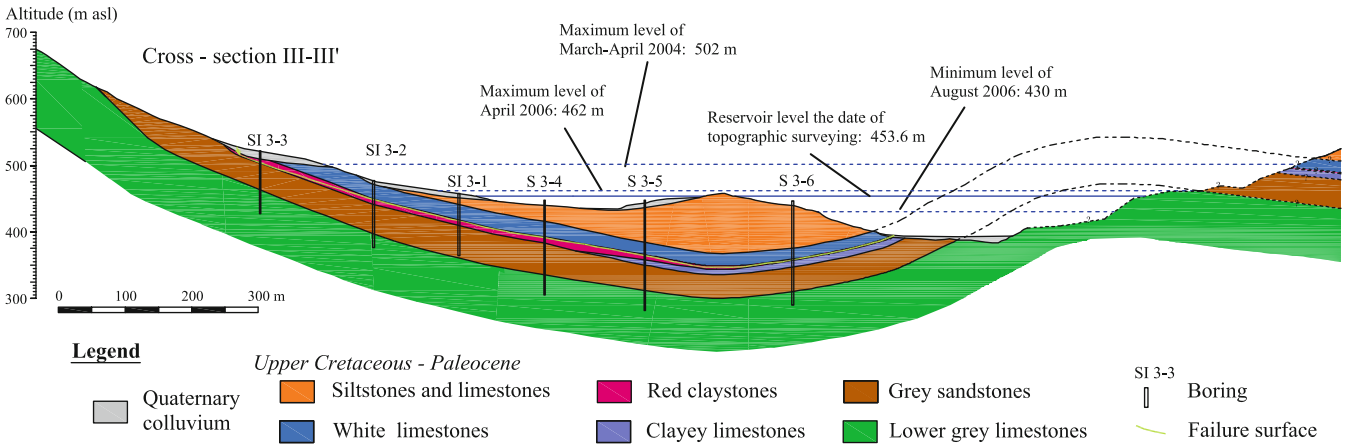

Fig. 13 Geological cross section III (see location in Fig. 5)

The set of the piezometer readings offers an interesting opportunity to calibrate the permeability of the main geological units of the landslide. This is a first step towards the analysis of failure conditions.

Pore water pressure calculation

The characterization of the slide, the laboratory tests performed and the piezometric measurements seem to indicate that the cause of the sliding was the high water pressures that remained within the low permeability Garumnian clayey layer, together with the absence of the stabilising effect of reservoir water due to the drawdown. Rapid drawdown is a complex problem which integrates unloading of the reservoir's water weight, soil deformation and water flow under saturated/unsaturated conditions. It has been discussed in Pinyol et al. (2008).

The analysis presented here was carried out by means of the finite element code Code_Bright, which can solve coupled flow/deformation problems in saturated/unsaturated media. The theoretical background of Code_Bright is described in Olivella et al. (1996), DIT-UPC (2002) and Pinyol et al. (2008). Alonso et al. (2005, 2011) report the application of Code_Bright to earth and rockfill dam analysis. These papers provide an account of the characteristics and capabilities of the code.

The model geometry used for finite element calculations is shown in Fig. 20. It corresponds to cross section II (Fig. 12). The

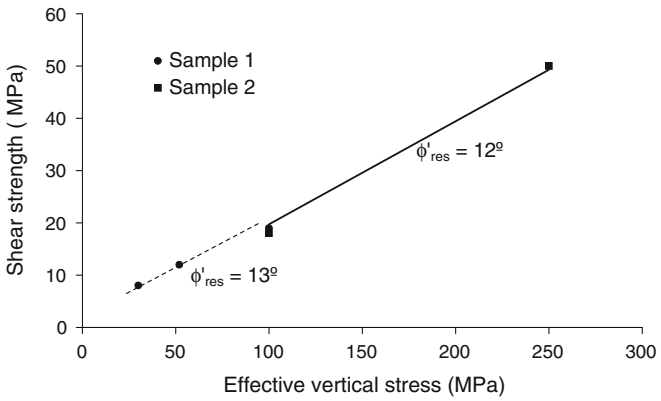

Fig. 14 Residual frictional strength obtained in ring shear test on remoulded Garumnian clay specimens

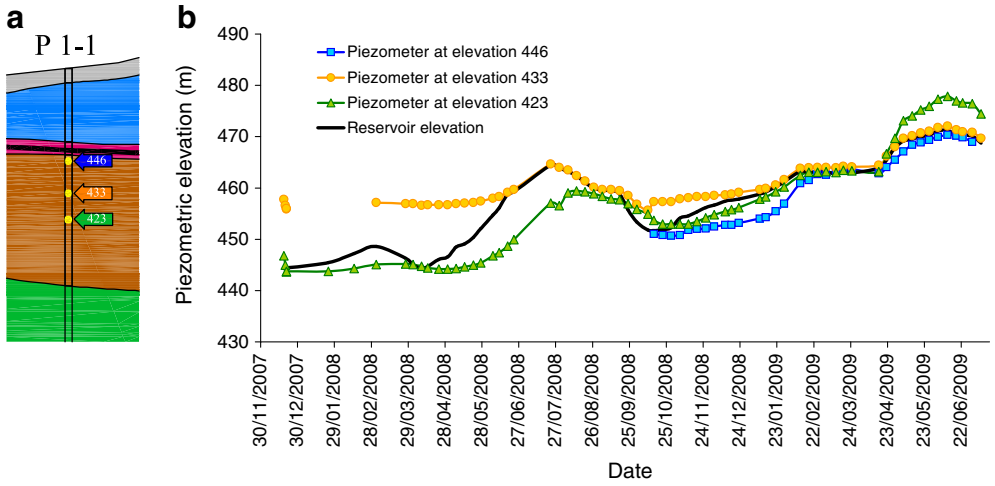

Fig. 15 **a** Position of piezometers in borehole P 1-1 (see Fig. 5); **b** piezometer records and reservoir elevation

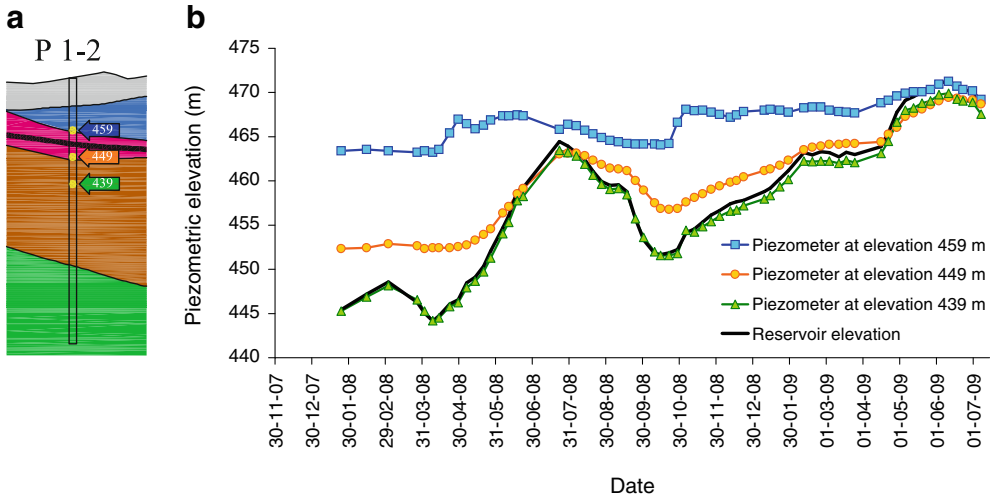

Fig. 16 **a** Position of piezometers in borehole P 1-2 (see Fig. 5); **b** piezometer records and reservoir elevation

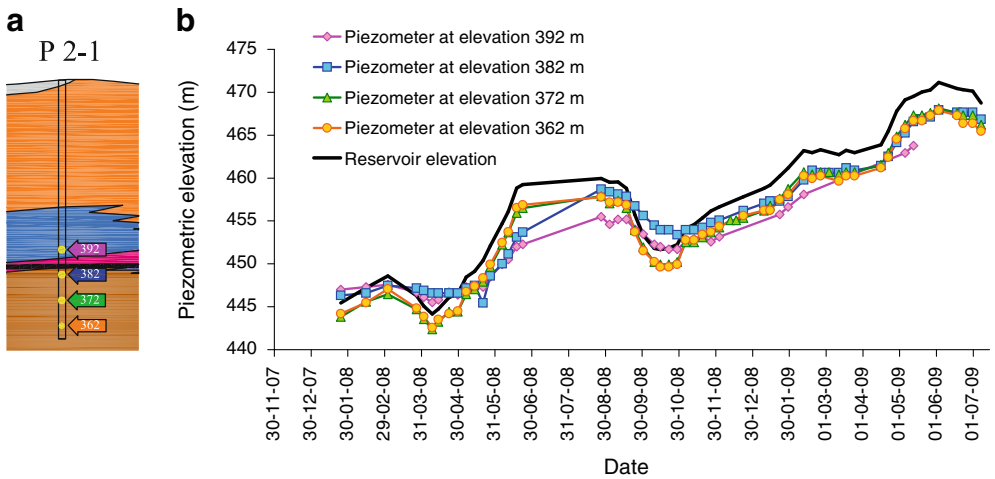

Fig. 17 **a** Position of piezometers in borehole P 2-1 (see Fig. 5); **b** piezometer records and reservoir elevation

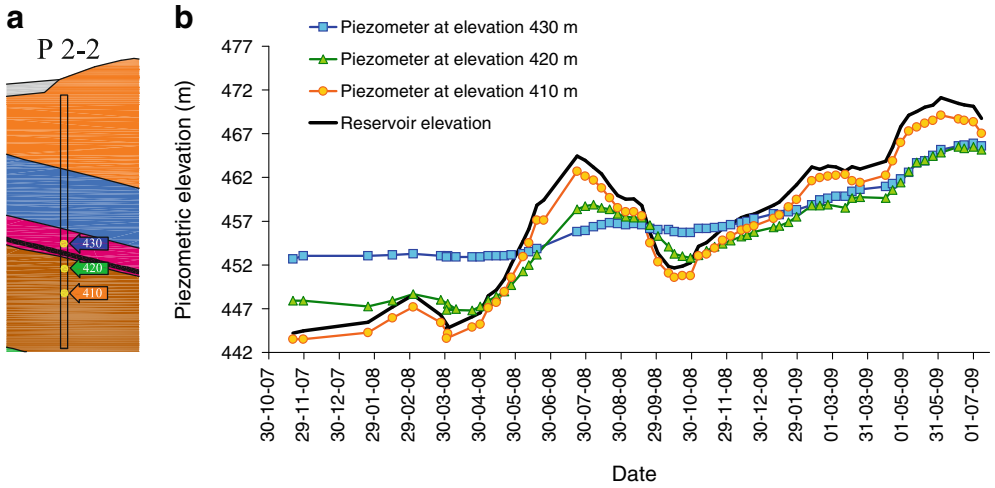

Fig. 18 **a** Position of piezometers in borehole P 2-2 (see Fig. 5); **b** piezometer records and reservoir elevation

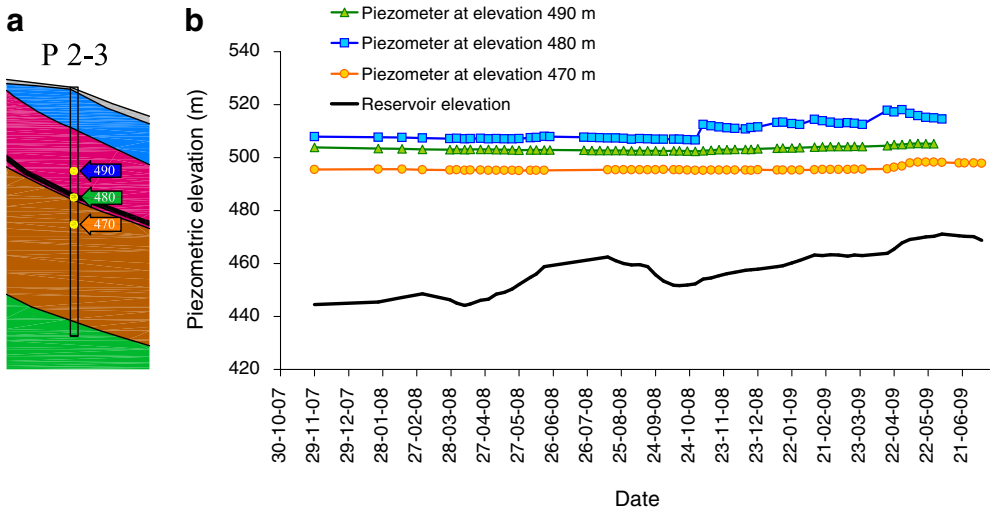

Fig. 19 **a** Position of piezometers in borehole P 2-3 (see Fig. 5); **b** piezometer records and reservoir elevation

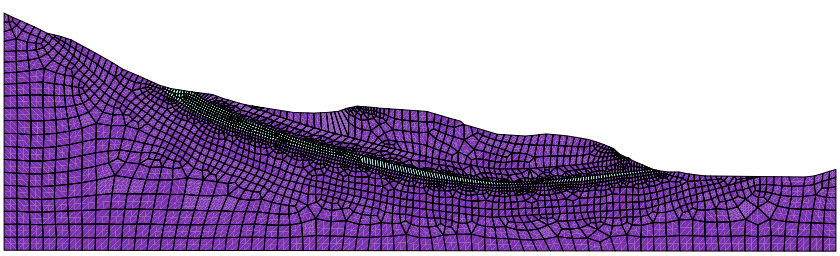

Fig. 20 Finite element model of cross section II (Fig. 12)

Table 1 Parameters for coupled hydro-mechanical calculations

Parameter and unit	Clay	Rock
Young's modulus (MPa)	500	2,500
Poisson's coefficient	0.3	0.3
Saturated permeability (m/s)	4.8×10^{-11}	10^{-5}
Van Genuchten parameters		
P_0	0.3	0.03
λ	0.33	0.33
$S_{r\ max}$	1	1
$S_{r\ max}$	0	0

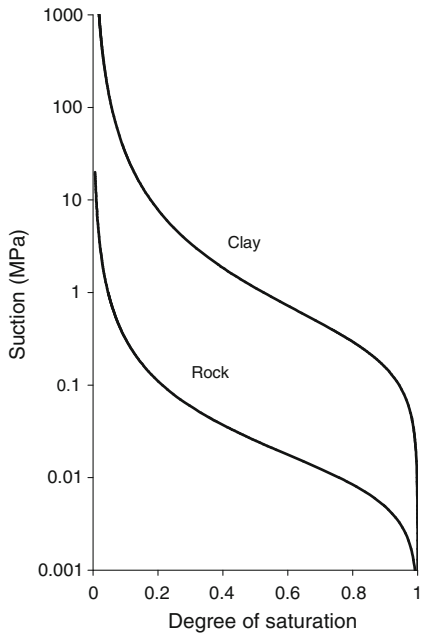

Fig. 21 Retention curves used in calculation

figure also shows a linear quadrilateral element mesh. Nodes have three degrees of freedom (water pressure and vertical and horizontal displacement). The mesh had to be refined mainly in the thinner clay layer to ensure the correct calculation of water flow through materials in direct contact having values of permeability widely different among them. In order to simplify the model, the sequence of detailed stratification above the Garumnian clay level has not been specified in detail. The mobilised rock above the clay mainly consists of siltstone and limestone layers.

The stress–strain behaviour of the materials was characterized by means of a linear elastic law defined by Young's modulus and Poisson's ratio. This simplification was thought to be acceptable for the objective of hydrological calibration of the model. In fact, elasto-plastic considerations have limited effect when estimating drawdown-induced pore water pressure. This result was discussed in Pinyol et al. (2008) and it is explained because the drawdown mainly results in an elastic stress path. In addition, the involved materials are highly overconsolidated rocks. Thus, the elastic hypothesis seems sufficient in this case. Table 1 shows the elastic values chosen, as well as the saturated permeability. Clay permeability was derived from laboratory tests. Other parameters were estimated according to typical values due of lack of precise data.

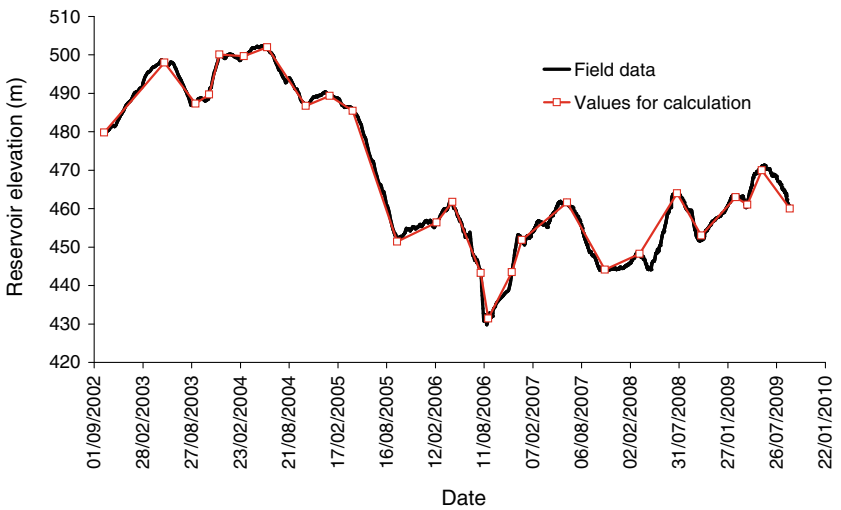

Fig. 22 Time variation of reservoir level

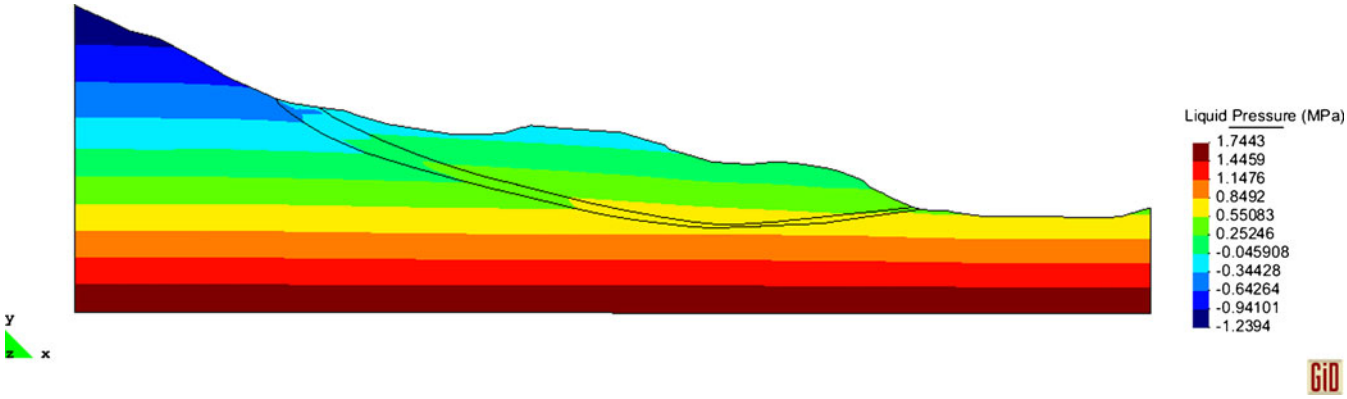

Fig. 23 Calculated pore water pressure distribution on September 26, 2005 when reservoir elevation was at 451 m

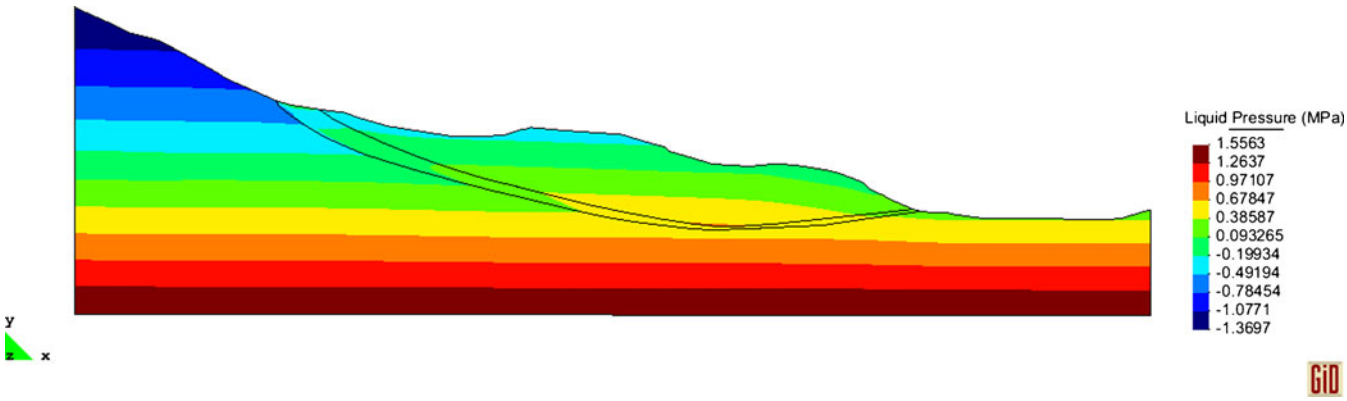

Fig. 24 Calculated pore water pressure distribution on August 21, 2006 when reservoir elevation was at 431 m

The analysis requires the characterization of materials under unsaturated conditions. The retention curves introduced in the calculations use the Van Genuchten model having the parameters indicated in Table 1 and plotted in Fig. 21. Relative permeability is defined according to the cubic law ($k = k_{sat} k_{rel} = k_{sat} S_r^3$ where k_{sat} is the saturated permeability and S_r is the degree of saturation) for both materials.

The known history of water level elevation was modelled during the 4 years prior to the drawdown that probably caused the failure and it was then continued until July 2009 (Fig. 22). This allows establishing the pressures acting on the failure surface with the purpose of analysing the stability at any time. In addition, the measurements taken in the piezometers installed in November 2007 could be compared with calculations in an effort to validate the numerical model. The initial pore water pressure assumed in the calculation is a horizontal hydrostatic profile.

The effect of rainfall has been incorporated in the simulation in order to model the yearly water inflow through the upper part of the slope, which is equal to the mean annual precipitation recorded in the region (400 mm).

Figures 23 and 24 show the water pressure contours calculated for 26th September 2005 and 21st August 2006, when water elevation of the reservoir reached 451 and 431 m. This last elevation corresponds to the minimum value reached in the period 1986–August 2006. The effect of the low permeability of the clay layer and its continuity can be observed by the abrupt change of the contours. This can be clearly observed in Fig. 25, which shows the calculated pore water pressure along a vertical cross section located in the position of P 2-2.

The pore water pressure distribution given in Figs. 23 and 24 has been introduced in the calculation of the safety factors by means of a

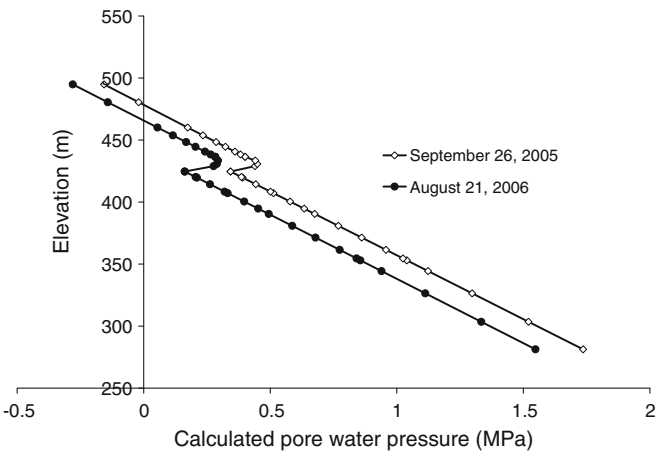

Fig. 25 Calculated pore water pressure distribution along the vertical profile located at the position of SI 1-2 (see Fig. 5) on September 26, 2005 and August 21, 2006 when reservoir elevation was at 451 and 431 m, respectively

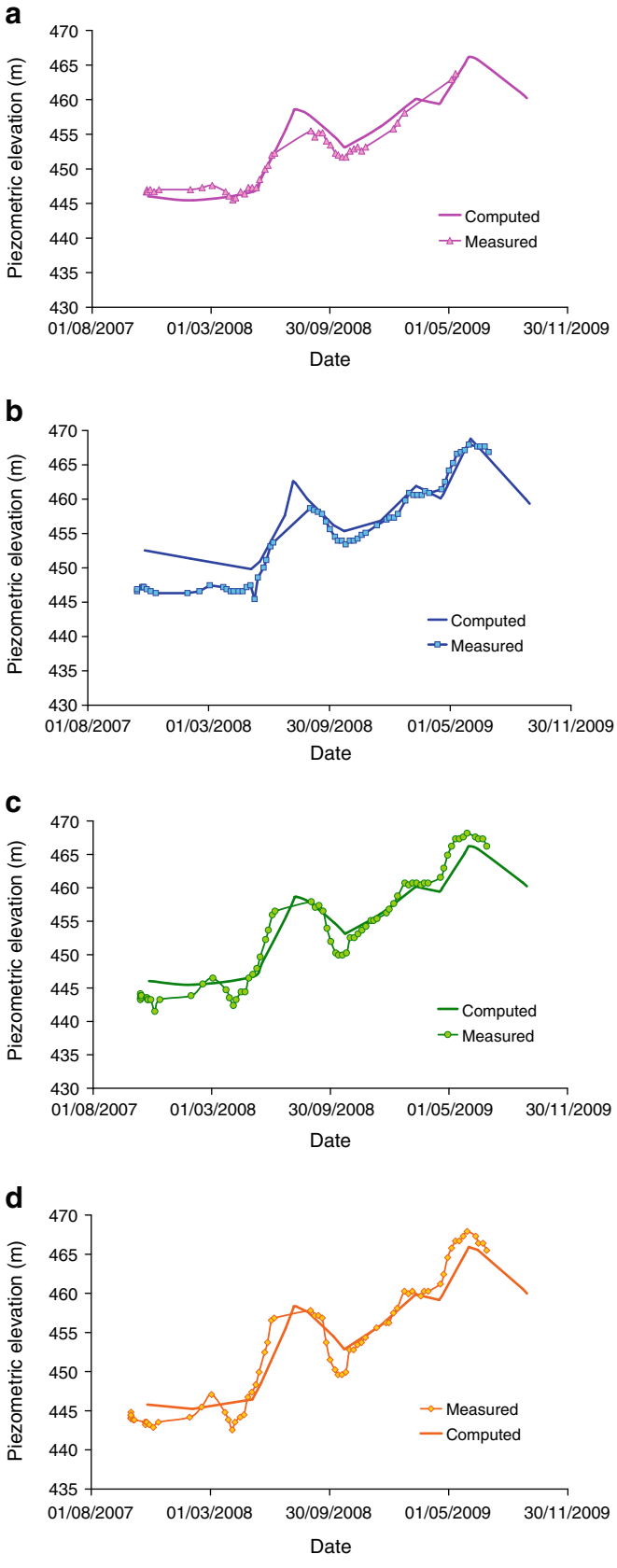

Fig. 26 Comparison of calculated and measured pore water pressure in piezometers located in boring P 2-1 at elevation **a** 392 m, **b** 382 m, **c** 372 m and **d** 362 m

limit equilibrium procedure and the Morgenstern–Price method to analyse the stability in the most critical situations previous to the failure.

However, before the analysis of the failure is presented, the calculated pore water pressure will be compared with piezometer measurements recorded after the failure in order to check the reliability of results. Figures 26, 27 and 28 show such comparison for the piezometers installed in cross section II (see their position in Figs. 5, 17a, 18a and 19a).

Pore water pressures measured within the lower sandstone in P 2-1 and P 2-2, which follow precisely the reservoir elevation evolution, are well captured by the calculation. This is a consequence of a correct choice for sandstone permeability. Pressure measurements within the

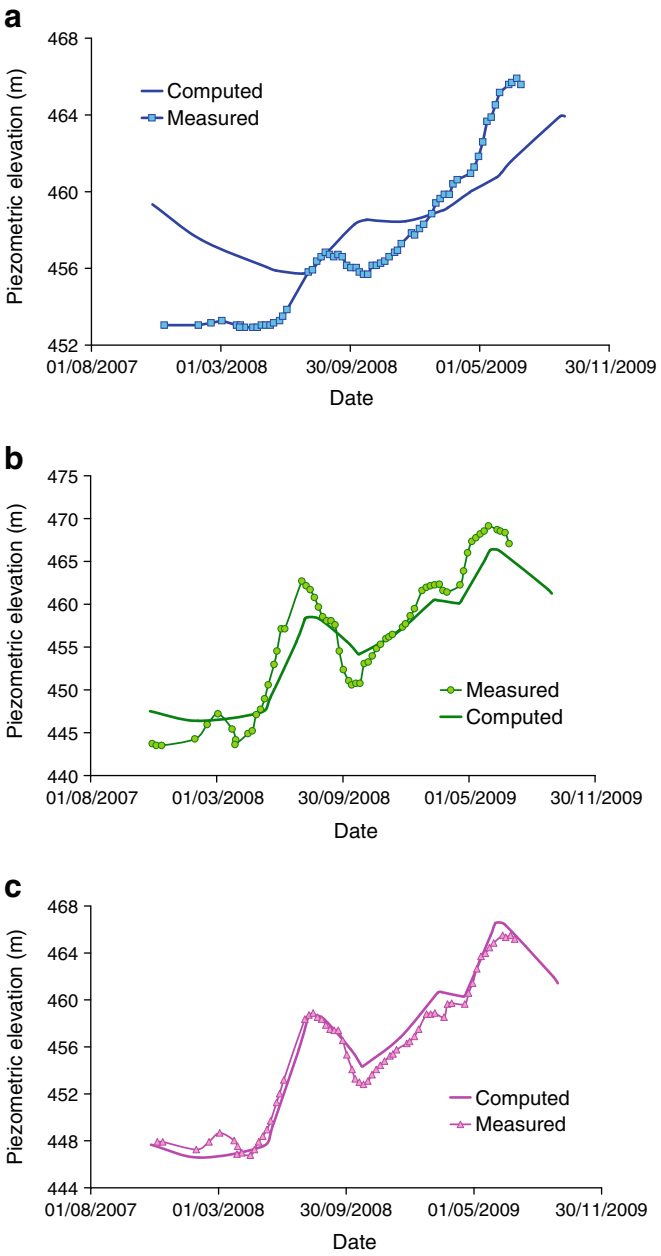

Fig. 27 Comparison of calculated and measured pore water pressure in piezometers located in boring P 2-2 at elevation **a** 430 m, **b** 420 m and **c** 410 m

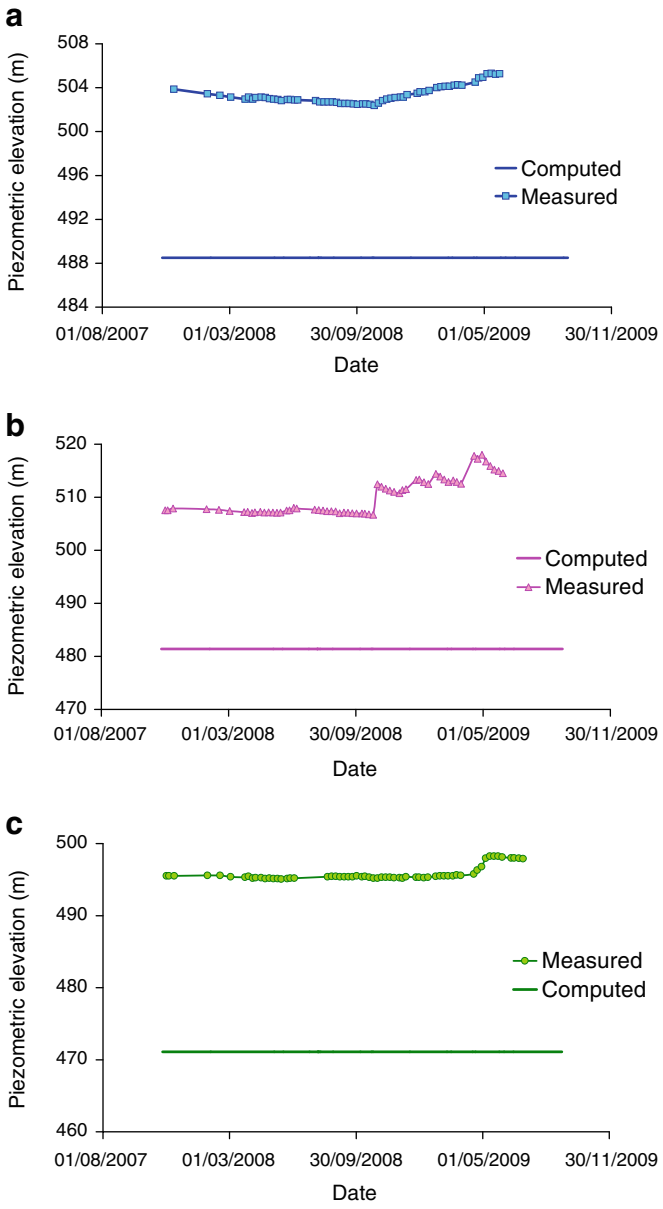

Fig. 28 Comparison of calculated and measured pore water pressure in piezometers located in boring P 2-3 at elevation **a** 489.87 m, **b** 480.07 m and **c** 469.87 m

impervious clayey layer in P 2-2, which are especially important for the subsequent calculation of safety factor, have been simulated quite satisfactorily. Pressures are lightly overestimated when the reservoir reaches low levels.

The main discrepancy appears in piezometer sensors installed at P 2-3 (Fig. 12). Field measurements show water columns in excess of 15–25 m over the sensors location. Instead, in our calculations, no positive pore water pressures above the piezometer positions are obtained because reservoir levels are always below the elevation of piezometer sensors and permeability of sandstone allows a rapid infiltration towards the reservoir. High pressures observed in the sensors might be the consequence of a perched water table fed by groundwater inflow from upslope.

Landslide stability safety factor

The failure surface was interpreted to be located entirely within the red claystone unit (Garumnian facies), as it was aforementioned. Therefore, once the landslide geometry is fixed, the limit equilibrium analysis only requires the definition of the average soil unit weight above the failure surface, the strength properties of clay, the pore water pressure acting on the failure surface and the landslide geometry. The unit weight of the mobilised mass has been estimated equal to 21 kN/m^3.

The strength available on the failure surface was defined by a Mohr–Coulomb law. Since the slide is the reactivation of an ancient slide, the residual angle and a null effective cohesion should be used. As it is mentioned in "Geomechanical and hydraulic properties of the Garumnian clay", the ring shear tests carried out in the laboratory and the associated discussion let to estimating a residual friction angle in the range of 10–12°. Both values will be considered in the calculations.

In the limit equilibrium model, the failure surface has been predefined following the geological interpretation. Pore water pressure on the failure surface is imposed following the results obtained previously in the coupled analysis (results given in Figs. 23 and 24). The increase in strength due to suction was neglected in the unsaturated area.

The two critical drawdown events (September 2005 and August 2006) have been analysed. The safety factors obtained are indicated in Table 2 for two clay friction angles, 10° and 12°. The values obtained for $\phi'=10°$ are very close to 1. Both drawdown situations were quite critical. However, the calculated safety factors are higher than 1 in both cases. Several factors can explain this discrepancy. It is uncertain if the analysed section is the most critical one. On the other hand, piezometer measurements indicate higher pore water pressure values in the upper part of the landslide. They were not introduced in the analyses summarized in Table 2. If piezometer values are introduced in the limit equilibrium analysis, maintaining unchanged the remaining parameters and conditions, a safety factor equal to 1.01 is obtained for the situation in August 2006. It is concluded that the failure was a result of the rapid drawdown and the low water level reached in the reservoir.

A low elevation of the reservoir level was also recorded in the summer of 1991 after a drawdown similar than the one

Table 2 Safety factors calculated by limit equilibrium analysis

	26 September 2005. Reservoir elevation 451 m	21 August 2006. Reservoir elevation 431 m
$\phi'=12°$	1.25	1.31
$\phi'=10°$	1.04	1.09

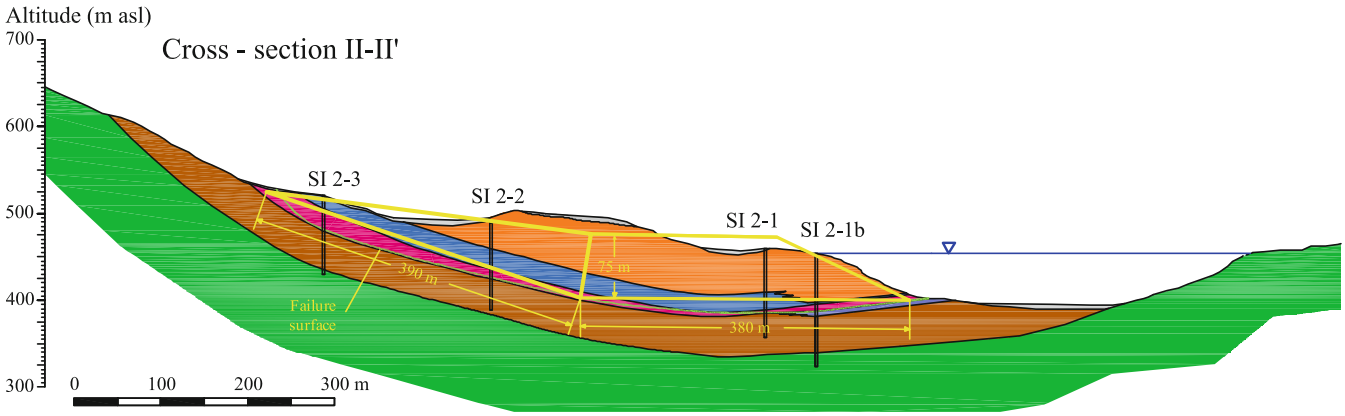

Fig. 29 Calculation section considered for the thermo-hydro-mechanical analysis (legend as in Fig. 12)

occurred in 2006 (Fig. 2). However, no evidences of landslide movement were detected in 1991. This fact may be explained if the previous histories of the reservoir level of the two events are compared. Previous to the drawdown in 1991, water reservoir level remained at a relatively higher elevation (higher than 480 m) during a short period of time compared with the long period (more than 8 years) previous to the drawdown in 2006. Taking into account the low permeability of the clay, pore water pressure at that layer, when the drawdown started in 1988, was probably lower than the value acting in 2003. As a consequence, the negative effect of the drawdown in 1991 was less critical than the drawdown in 2006, which led to the failure of the slope. In addition, the average velocity of the drawdown in 1991 was somewhat lower and the minimum reservoir level remained 2 m higher than the level reached in 2006.

The risk of rapid sliding

An additional risk is the possibility of rapid sliding which will result in the impact of the sliding mass against the reservoir water and the subsequent generation of uncontrolled destructive waves. A clear reference is the Vaiont slide in northern Italy in 1963. The phenomena that may lead to this rapid acceleration were discussed in Pinyol and Alonso (2010a, b). The coupled thermo-hydro-mechanical problem has been solved in a representative cross

Table 3 Physical constants and properties

Parameters	Symbol	Value	Unit
Water			
Density	ρ_w	1,000	kg/m^3
Compressibility coefficient	α_w	5×10^{-10}	1/Pa
Thermal expansion coefficient	β_w	3.42×10^{-4}	1/ºC
Specific heat	c_w	4.186×10^{3}	J/kg °C
		1.0	cal/kg °C
Solid particles			
Density	ρ_s	2,700	kg/cm^3
Thermal expansion coefficient	β_s	3×10^{-5}	
Specific heat	c_s	8.372×10^{2}	J/kg ºC
		0.20	cal/kg ºC
Shearing band			
Porosity	n	0.2	–
Permeability	k	4.9×10^{-11}	m/s
Compressibility coefficient	m_v	2.1×10^{-9}	1/Pa
Friction angle (residual)	ϕ	10	º
Landslide material			
Density	ρ_r	2,200	kg/m^3

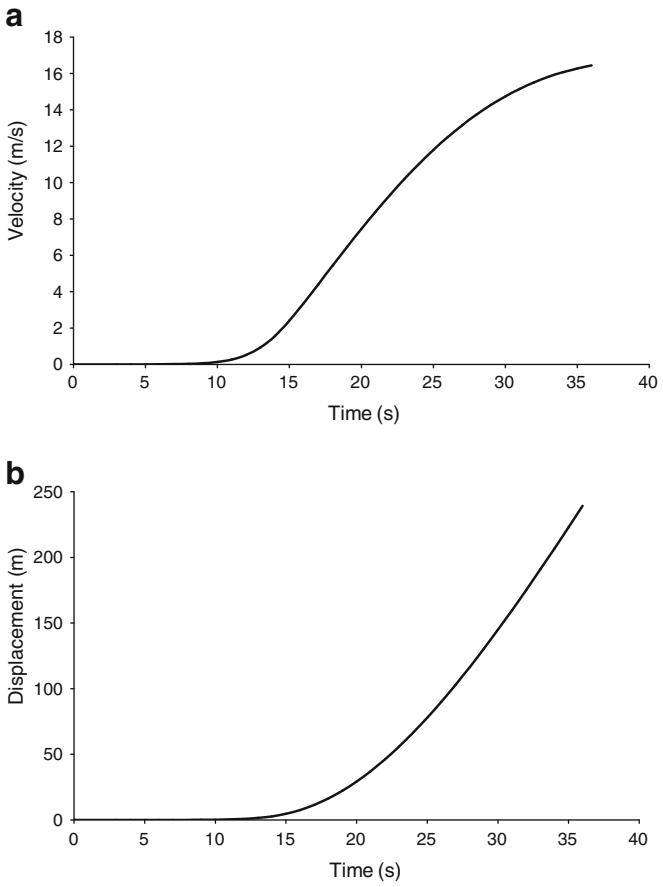

Fig. 30 Calculated evolution of the sliding velocity and displacement considering the thermo-hydro-mechanical effects

section of the Canelles landslide consisting of two blocks of varying mass. The failure surface was simplified by means of two planes: one under the upper block, which dips 18°, and another one under the lower block, next to the reservoir, which is horizontal (Fig. 29). This geometry allows taking into consideration the increasing slide stability as the slide progresses towards the reservoir. In fact during sliding, the soil mass increases in the more stable lower block and decreases in the unstable upper block.

The analysis requires the specification of some thermo-hydro-mechanical properties of the clay layer, where the failure surface is located. Table 3 provides the calculation parameters. The values selected for water and solid particles correspond to well-accepted values found in handbooks of physico-chemical constants.

At this point, it is necessary to consider the existence of a shear band of some thickness where the shearing strains develop on the basal sliding surface. The specific properties of the shearing band material (Garumnian clay) were defined previously. The coefficient of compressibility was calculated through the Young's modulus used previously (500 MPa) and ν=0.3. It is difficult to estimate accurately the thickness of the shearing band, even if recovered samples are examined. In general, the thickness of the shearing band is related to the size of the soil particles. In this case, the failure is located in a clayey soil having D_{50}=0.01 mm (aperture diameter of the mesh through which 50% of the material passes). For this value, a thickness of 5 mm is estimated for the shearing band.

The position of the reservoir level considered for this calculation corresponds to the critical situation after the occurrence of the actual drawdown, when the reservoir elevation was 430 m. The pore water pressure distribution on the clay layer under the lower block has been simplified to be a constant averaged value of the actual pore water pressure distribution which brings the slide to strict equilibrium. The movement is then triggered by increasing in 1 kPa the pore water pressure on the failure surface of the lower block. The actual value of the increment in pore pressure does not have any significant effect in this part of the analysis. The idea here is simply to initiate the motion so that the thermal processes begin to operate. Once the motion starts, the memory of the triggering mechanism is soon lost.

Figure 30 shows the calculated evolution of the slide velocity during a displacement of 250 m. According to calculations, the slide would accelerate, reaching 16 m/s in a few seconds. At the beginning, the sliding velocity remains low, close to a few millimetres per second. During the first seconds, the excess pore pressure accumulated in the shear band is not enough to significantly reduce the effective frictional strength.

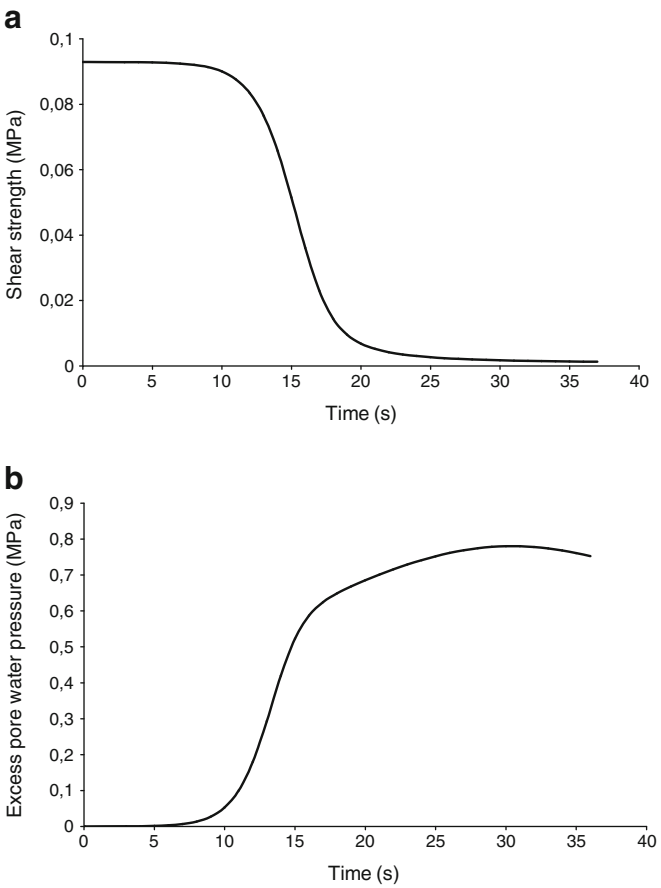

Fig. 31 Evolution of **a** the frictional effective strength and **b** water pressure in the failure surface under the lower block

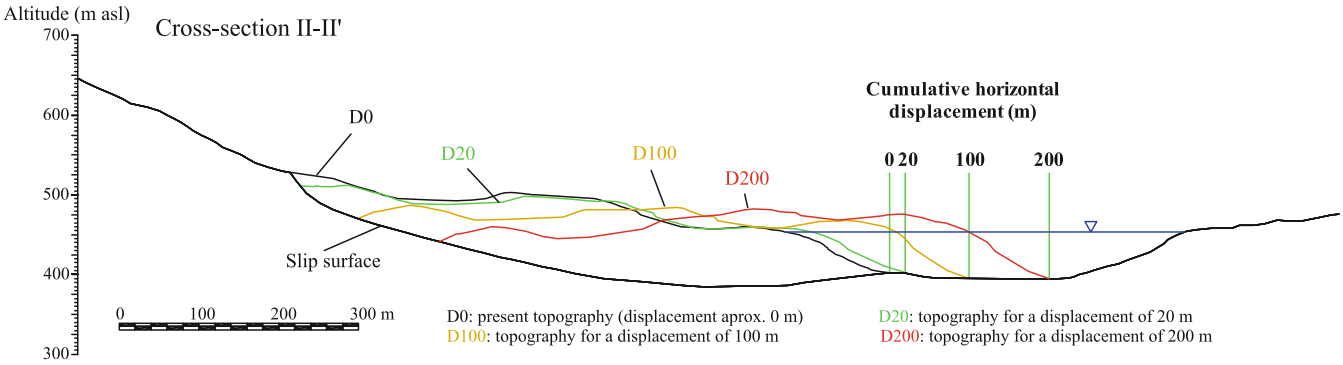

Fig. 32 Simulated movement of the landslide mass for several displacement increments. The simulation was made considering conservation of the cross-sectional area of the moving mass during displacement

Figure 31 shows the evolution of strength and the excess in water pressure during the same period of time. When pore pressure in the shear band increases (up to 0.8 MPa), shearing strength decreases and drops to values close to 0. This explains the high velocities reached by the slide.

If the effects of heat are neglected, the maximum velocity reached by the slide becomes significantly lower (2 mm/s). In this case, at t=40 s, the slide would stop, after travelling 4.5 cm towards the reservoir.

The preceding calculation provided the necessary data to plot the theoretical displacement in time of the slide. This is shown in the sequence of landslide positions plotted in Fig. 32. The geometry refers to cross section II which is the most representative of the slide. This series of plots allows a subsequent calculation of the waves generated in the reservoir, a subject which is outside of the scope of the paper. In the wave calculation performed, the landslide was simplified as a 3D block, 1,100 m wide, whose evolving uniform cross section is given in Fig. 32. The slide hits the opposite margin of the reservoir after 200 m of displacement.

The analysis of the sliding velocity has limitations because the resistance opposed by the water is not considered. However, in a fast motion, limited changes in the evolution of displacement (or velocity) in time have a reduced influence on the impact associated with the wave pattern generated. In the Canelles reservoir, the shoreline is essentially a non-populated zone and the main risk concerns the increased hydraulic thrust against the dam and the possibility of some overtopping.

Concluding remarks and corrective measures

The reactivation of a translational landslide about 40 Mm^3 located in the left margin of the Canelles reservoir, Spain, has been analysed. Geological and geotechnical investigations allowed the estimation of the position of the slide surface limited in the upper part by a continuous 2.5-km-long crack observed in the summer 2006 when the reservoir elevation was reduced. The slide surface has been located within a high plasticity clay layer of the Garumnian facies (Cretaceous–Paleocene transition). This clay layer, typically less than a dozen metres thick, was deposited between harder formations of sandstone (below) and limestones (above).

The first objective of the paper was to prove that the geometrical conditions of the landslide, reservoir level variations in the period 1996–2006 and the available frictional strength on the slide surface, as well as other relevant features of the materials (permeability), could explain the failure observed in 2006. In order to do that, a rigorous hydro-mechanical analysis referred to a representative central section of the landslide has been carried out. The time evolution of the reservoir level and an average rainfall have been introduced in the model developed.

The calculated pore water pressures, a fundamental aspect for the subsequent stability analysis of the landslide, have been compared to piezometer measurements recorded some months after the failure. The agreement is satisfactory and this result provides reliability to the analysis presented. A simple limit equilibrium analysis taking into account the calculated pore water pressure distributions at the time of the failure indicates that the reactivation of the Canelles landslide was mainly induced by the fast drawdown of August 2006.

Stability analysis of the slope for different reservoir elevations under the hypothesis of hydrostatic pore water pressure distribution defined by the reservoir level indicates that the slope is stable. The stability becomes critical when values of pore water pressure remain high within the slope in parallel with lower values of reservoir level. This is explained by the low permeability of the continuous clay layer. Three main reasons explain such high values of pore water pressure: direct rainfall contributions, underground flow from Blancafort Sierra and rapid drawdown phenomena. Only the third reason can be controlled in order to avoid the reactivation of the landslide. Additional sensitivity analysis in which drawdown of different intensities and velocities were modelled starting at a high water level (530 m, which is a critical situation for overtopping) indicated that the control of the drawdown was difficult to achieve in practice. According to the results, the stability could be guaranteed if drawdown velocity is limited to low values (around 0.15 m/day). This restriction impairs the correct operation of the reservoir.

On the other hand, an analysis to determine the risk of acceleration of the landslide has been developed taking into account the drop of effective shearing strength due to thermally induced pore water pressures in the sliding surface. The analysis indicates that the slide may reach a high velocity: 16 m/s in a few seconds. The non-accelerated motion of the slide and its subsequent stabilisation observed in the field cannot be explained with the theory applied here. However, this fact does not invalidate the conclusion that a risk of a strong slide acceleration exists. This is also discussed in

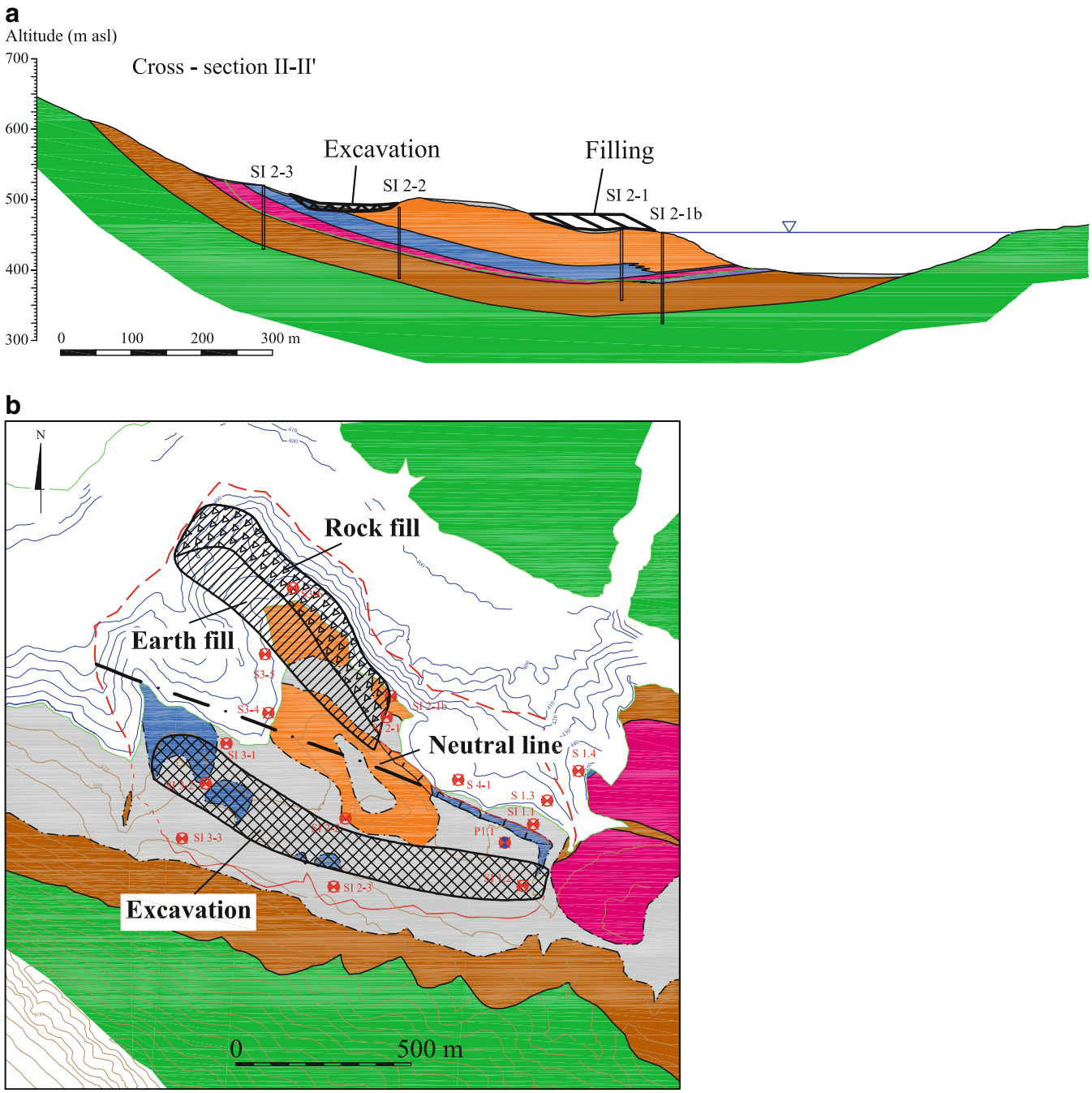

Fig. 33 Proposal of stabilisation by weight transfer: excavation and fill zones: **a** cross section II; **b** plan view (legend as in Figs. 5 and 12)

Vardoulakis (2002) and Pinyol and Alonso (2010a, b) for the well-known case of Vaiont.

The solution proposed for the stabilisation of the Canelles landslide in order to facilitate the operation of the reservoir is to modify the geometry by means of weight transfer from the upper part (active zone) to the lower part (passive zone). In order to determine the active and passive zones, the stability of the slope has been analysed varying the position of a vertical load along the slide. The variation of the safety factor with respect to an original situation (the case without load) has been evaluated. Positive increments of the safety factor define the passive zone, whereas negative increments indicated the active zone where the weight of the slope should be reduced. Figure 33 shows the proposal made. Excavation and filling zones for the weight transfer are defined. The weight transfer defined would increase the calculated safety factor of the Canelles slide in the case of rapid drawdown (v=1 m/day)

starting at elevation 450, to an estimated values of SF=1.25, which was considered acceptable.

Acknowledgements

This research work received partial support from the Safeland project funded by Commission of the European Communities (grant agreement 226479) and from the Big Risk (contract number BIA2008-06614) project funded by the Spanish Ministry of Science.

References

Alonso EE (2005) Parámetros de Resistencia en cálculos de estabilidad. *VI Simposio Nacional sobre Taludes y Laderas Inestables*. Valencia, 21–24 June 2005. Alonso E, Corominas J, Jordà L, Romana M and Serón JB (eds.), 1131–1195

Alonso EE, Gens A, Lloret A (1993) The landslide of Cortes de Pallas, Spain. Geotechnique 43(4):507–521

Alonso EE, Olivella S, Pinyol NM (2005) A review of Beliche dam. Geotechnique 55 (4):267–285

Alonso EE, Olivella S, Soriano A, Pinyol NM (2011) Modelling the response of Lechago earth and rockfill dam. Géotechnique 61(5):387–407

Corominas J, Moya J, Ledesma A, Lloret A, Gili JA (2005) Prediction of ground displacements and velocities from groundwater level changes at the Vallcebre landslide (Eastern Pyrenees, Spain). Landslides 2:83–96

CIMNEBarcelona, .DIT-UPC (2002) CODE_BRIGHT. A 3-D program for thermo-hydro-mechanical analysis in geological media. User's guide. CIMNE, Barcelona

Hutchinson JN (1983) Methods of locating slip surfaces in landslides. Bull Assoc Eng Geol 20:235–252

Hutchinson JN, Bhandari RK (1971) Undrained loading, a fundamental mechanism of mudflows and other mass movements. Geotechnique 21:353–358

Martínez Peña B, Pocoví A (1988) El amortiguamiento frontal de la estructura de la cobertera surpirinaica y su relación con el anticlinal de Barbastro-Balaguer. Acta Geol Hisp 23:81–94

Moya J (2004) Determination of the failure surface geometry in quick slides using balanced cross section techniques. Application to Aznalcóllar tailings dam failure. In: Hack R, Azzam R, Charlier R (eds) Engineering geology for infrastructure planning in Europe. Springer, Series Lecture Notes in Earth Sciences, no. 104, 414–421

Olivella S, Gens A, Carrera J, Alonso EE (1996) Numerical formulation for a simulator (CODE BRIGHT) for the coupled analysis of saline media. Eng Comput 13(7):87–112

Pinyol NM, Alonso EE (2010a) Criteria for rapid sliding II. Thermo-hydro-mechanical and scale effects in Vaiont case. Eng Geol 114(3–4):211–227

Pinyol NM, Alonso EE (2010b) Fast planar slides. A closed form thermo-hydro-mechanical solution. Int J Numer Anal Methods Geomech 34:27–52

Pinyol NM, Alonso EE and Olivella S (2008) Rapid drawdown in slopes and embankments. Water Resources Research 44, W00D03, 22 pp. Special issues on: Hydrology and mechanical coupling in earth sciences and engineering: interdisciplinary perspectives

Stark TD, Eid HT (1994) Slope stability analyses in stiff fissured clays. J Geotech Geoenviron Eng 123(4):335–343

Vardoulakis I (2002) Dynamic thermo-poro-mechanical analysis of catastrophic landslides. Geotechnique 52(3):157–171

Vergés J (1993) Estudi geològic del vessant Sud del Pirineu Oriental I Central: Evolució en 3D. PhD Thesis. Universitat Politècnica de Catalunya, Barcelona, Spain. 203p (printed by the Institut Cartogràfic de Catalunya in 1999)

N. M. Pinyol (✉) · E. E. Alonso · J. Corominas · J. Moya
International Center for Numerical Methods in Engineering, Department of Geotechnical Engineering and Geosciences,
Universitat Politècnica de Catalunya,
Edificio D-2, Campus Nord, UPC, 08034 Barcelona, Spain
e-mail: nuria.pinyol@upc.edu

N. M. Pinyol
Centre Internacional de Mètodes Numèrics en Enginyeria (CIMNE),
Universitat Politècnica de Catalunya,
Jordi Girona 1-3, Edifici C1, 08034 Barcelona, Spain